JACS
JOURNAL OF THE AMERICAN CHEMICAL SOCIETY
pubs.acs.org/JACS
Article

Rapid Mining of Fast Ion Conductors via Subgraph Isomorphism Matching

Wentao Zhang, Mouyi Weng, Mingzheng Zhang, Zhefeng Chen, Bingxu Wang, Shunning Li,* and Feng Pan*

Cite This: J. Am. Chem. Soc. 2024, 146, 18535−18543
Read Online
ACCESS | Metrics & More | Article Recommendations | Supporting Information

ABSTRACT: The rapidly evolving field of inorganic solid-state electrolytes (ISSEs) has been driven in recent years by advances in data-mining techniques, which facilitates the high-throughput computational screening for candidate materials in the databases. The key to the mining process is the selection of critical features that underline the similarity of a material to an existing ISSE. Unfortunately, this selection is generally subjective and frequently under debate. Here we propose a subgraph isomorphism matching method that allows an objective evaluation of the similarity between two compounds according to the topology of the local atomic environment. The matching algorithm has been applied to discover four structure types that are highly analogous to the $LiTi_2(PO_4)_3$ NASICON prototype. We demonstrate that the local atomic environments similar to $LiTi_2(PO_4)_3$ endow these four structures with favorable Li diffusion tunnels and ionic conductivity on par with those of the prototype. By further taking into account the electronic structure and electrochemical stability window, 13 compounds are identified to be potential ISSEs. Our findings not only offer a promising approach toward rapid mining of fast ion conductors without limitation in the compositional range but also reveal insights into the design of ISSEs according to the topology of their framework structures.

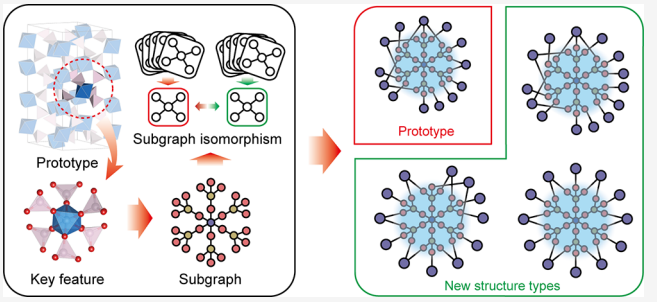

1. INTRODUCTION

Lithium-ion batteries are widely accepted as an enabler of electric vehicles and smart electricity grids equipped with renewable energy sources.[1,2] While enormous improvements have been made with regard to their energy density, power capability, and cycle life, an intense quest for battery materials that can enhance operational safety is still underway. All-solid-state lithium-ion batteries using inorganic solid-state electrolytes (ISSEs) could not only avoid the flammability issue of conventional liquid organic electrolytes but also offer additional advantages such as the compatibility with a Li metal anode, the absence of leakage and a potentially wider electrochemical stability window.[3] A considerable number of fast ion conductors[4−10] have already been explored as ISSEs, some of which show a promising ionic conductivity exceeding 10^{-3} S/cm at ambient temperatures.[11] Nevertheless, the majority of previous efforts have been based on trial-and-error experiments, while the rest have relied on expensive high-throughput first-principles calculations. Moreover, the proposed design principles are generally limited to specific compositions and structures. In this sense, it is still a challenge to formulate a strategy that can accelerate the discovery of ISSEs both in a cost-effective way and without limitation in the compositional range.

Data mining in the materials databases has been proposed to serve as a viable preprocessing step for the search of fast ion conductor materials.[10,12−14] Early studies focused on the identification of certain Li environments appropriate for diffusion,[15] while others tried to examine the arrangement of non-Li atoms,[3,16−18] since the rigid non-Li framework can to a large extent determine the efficiency of ionic transport in the Li percolation pathways.[19] Specifically, it was demonstrated that the anion arrangement is directly responsible for the mode of Li migration and can be used as a criterion for discovering sulfide fast ion conductors.[3] Yet, since O ions are relatively smaller than S ions and less polarizable than the latter,[11] the ability of interatomic screening that decreases the influence of non-Li cations on Li diffusion is considerably weaker for O ions than that of the S counterpart.[20] This makes any criterion focused on anion arrangement hardly applicable for oxide ISSEs, while oxide ISSEs are indeed more preferable for Li ion batteries owing to their higher air and electrochemical stability.

Received: March 28, 2024
Revised: June 18, 2024
Accepted: June 20, 2024
Published: June 28, 2024

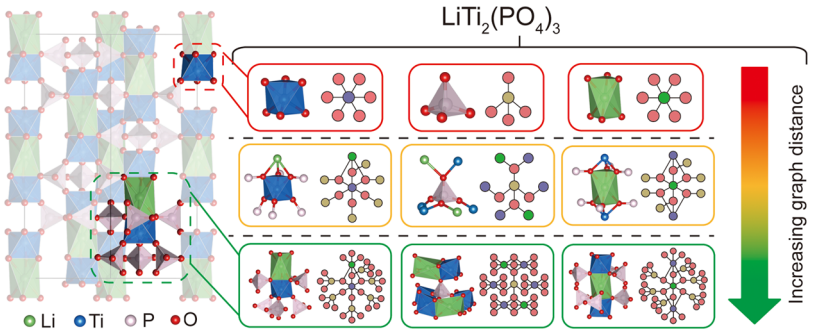

Figure 1. Crystal structure converted into subgraphs. The NASICON phase of $LiTi_2(PO_4)_3$ can be described by five subgraphs with Li, Ti, P, and O as the central atoms (O has two types of subgraphs). Only the subgraphs of the cation centers are shown here. The graph distance indicates the minimum number of edges between two nodes along the neighborhood relations. Subgraphs with a graph distance of three (green frames) contain the information on how the neighboring polyhedra (graph distance of one, red frames) are topologically linked to the central one. Color code of the atomic structures: Li, green; O, red; Ti, blue; and P, pink. For clarification, the color of the P atom in the subgraph representation (dark yellow) is different from that in the atomic structures.

Human intuition says that compounds with a similar structure to existing ISSEs are more probable to exhibit a high ionic conductivity. Therefore, structure matching algorithms, potentially with respect to the spatial symmetry of the crystal structure, the coordination number of atoms and the Wyckoff sites, etc.,[21] can be employed for materials screening. This approach was previously developed via an atom-by-atom displacement comparison with a standardized cell.[22] Despite their accuracy, such global structural descriptors tend to fall short in gauging the similarity of local atomic environments, not to mention that the screening criteria are generally subjective. To overcome these limitations, we herein design a graph-based algorithm, which can accurately interpret the interatomic connection and enable an objective and convenient evaluation of the similarity between two compounds according to the topology of the local atomic environment. This algorithm can provide a new avenue for the recommendation of potential fast ion conductors for ISSEs.

The algorithm proposed in this work is based on subgraph isomorphism matching from the graph theory. We have chosen $LiTi_2(PO_4)_3$ as the prototype material for the exploration of potential ISSEs. $LiTi_2(PO_4)_3$ has a NASICON-type structure, in which a framework of combined octahedral (Oct) and tetrahedral (Tet) coordination environments is critical for the construction of facile Li diffusion pathways.[23−25] With our graph-based algorithm, four structure types that are highly analogous to $LiTi_2(PO_4)_3$ have been discovered. First-principles calculations further justify that they have Li diffusion activation barriers on a similar scale to that of $LiTi_2(PO_4)_3$. A detailed comparison between the corresponding compounds suggests that the direct Oct−Oct Li diffusion paths can contribute to a barrier lower than that of the prototype material. A series of potential ISSEs are thus identified, with both a room-temperature ionic conductivity reaching the order of 10^{-2} S/cm and an electrochemical stability window of over 2 V.

2. RESULTS

2.1. Graph Representation of Atomic Environments.

The crystal structure of a compound can be translated into an undirected graph with atoms as vertices and atomic connection relationships (i.e., chemical bonds) as edges. To further consider the local atomic environment and the periodic boundary conditions of crystal structure representation, all of the atoms in the cell are traversed and a subgraph is generated based on the neighbors of the selected atom.[26−28] An area−distance pair clustering method was used to determine the atomic connection relationships (details are provided in the Supporting Information), which facilitates a reliable extraction of the local atomic environment.

The subgraph representation of $LiTi_2(PO_4)_3$ is displayed in Figure 1. The basic coordination environments include LiO_6 and TiO_6 octahedra and PO_4 tetrahedra, which correspond to a graph distance of one (red frames). When atoms of the outer sheath of these polyhedra are considered, they correspond to a graph distance of two (yellow frames). Then, a subgraph with a graph distance of three (green frames) contains a central polyhedron and its neighboring polyhedra (e.g., a central TiO_6 octahedron with its neighbors including six PO_4 tetrahedra and one LiO_6 octahedron). Subgraph isomorphism is defined as a bijection between both the node sets and edge sets of two subgraphs, which indicates the similarity between two crystal structures.

We note that subgraph isomorphism does not necessarily imply the complete matching of two structures. While the topology of the local atomic environment is the same, the detailed alignment of the polyhedra could be different, leading to a fine distinction between the subgraphs on a larger scale. For example, there are cases where two structures exhibit the same subgraph with a graph distance of up to three but they show different subgraphs with a graph distance of four. In fact, previous studies have already revealed that the polyhedral models of non-Li cations are the key structure units dictating the Li ion transport in ion conductors.[29] A polyhedral module connection algorithm was recently developed for the exploration of fast ion conductors, employing corner-sharing descriptors between two non-Li units.[20] However, in these studies, only the type of connection between polyhedra was considered, which is definitely not enough to interpret the similarity between two structures and therefore requires substantial high-throughput first-principles calculations for further screening. Our subgraph isomorphism algorithm can offer significant improvement over the previous ones by taking into account the overall topology of the non-Li framework. Finding structures with a similar topology of local atomic environment to an existing ISSE would likely provide a better chance of finding a similar structure of Li diffusion tunnels. This enables us to narrow down the range of searches and

https://doi.org/10.1021/jacs.4c04202
J. Am. Chem. Soc. 2024, 146, 18535−18543

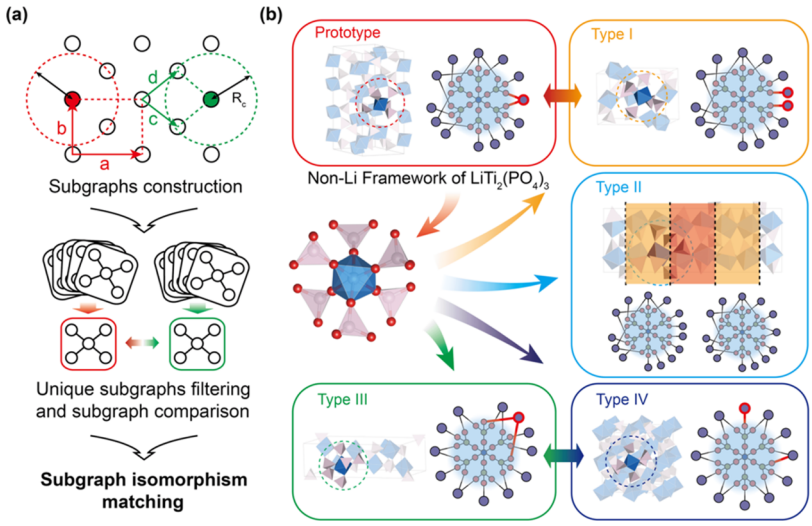

Figure 2. Subgraph isomorphism matching process and the four structure types identified as similar to the $LiTi_2(PO_4)_3$ prototype. (a) Flowchart of the subgraph isomorphism matching method. (b) Local atomic environments of the four structure types that are topologically related to the $LiTi_2(PO_4)_3$ prototype. The subgraphs with a graph distance of three (indicated by the blue shadow) are the same among these structure types and the prototype. Difference emerges in the subgraphs with a graph distance of four with the distinctive nodes highlighted by red circles.

reduce the cost of high-throughput calculations. Moreover, it could also yield insights into how specific environments of Li diffusion tunnels affect the ionic conductivity, as will be discussed in the following sections.

2.2. Subgraph Isomorphism Matching for $LiTi_2(PO_4)_3$. The subgraph isomorphism method only captures the information on topology and does not consider the elements of the constituent atoms.[26] For two identical crystal structures that adopt different unit-cell-axis directions, as shown in Figure 2a, their constructed subgraphs are actually the same, and the algorithm inspects all subgraphs and finally specifies that their local structures are isomorphic. For two different crystal structures, the bijective mapping between their corresponding subgraphs with a graph distance of up to three will indicate the similarity between these structures. Subgraph construction, unique subgraph filtering, and bijective alignment are conducted in a parallel fashion to facilitate efficiency in the matching process.

Using the NASICON structure of $LiTi_2(PO_4)_3$ as a prototype, four structure types are discovered to share the same topology of the local atomic environment as $LiTi_2(PO_4)_3$, as shown in Figure 2b. For the sake of clarity, only the subgraphs with Ti at the center node are depicted. A bijective mapping between unique subgraphs with a graph distance of four was conducted to group the structures with an identical set of subgraphs into the same category. Structure type I, in the $P2_1/c$ space group, has a $[MO_6]_2[XO_4]_3$ (M is a metal atom and X is a main group element) configuration which is identical to $LiTi_2(PO_4)_3$ but shows different alignments along the *c*-axis. The prototype has a linearly aligned configuration while the structure type I shows a zigzag alignment.[23] We note that structure type I has been previously reported to be characteristic of a stable framework and promising ion mobility, and can thus be employed as cathode[30−32] or ISSE[23] materials. Structure type II, belonging to the *Pbca* space group, features two distinct $[MO_6]_2[XO_4]_3$ alignments separately, one corresponding to the prototype and the other corresponding to the structure type I. Structure type III, in the $Ia\bar{3}d$ space group, closely resembles the garnet structure of $Li_3Ln_3Te_2O_{12}$[33] and $Li_5Ln_3Nb_2O_{12}$,[34] a famous group of ISSEs with high ionic conductivity. In these phases, Li ions diffuse through the Oct and Tet sites sequentially in a flattened energy landscape.[33] Structure type III has the same space group as $Li_3Ln_3Te_2O_{12}$ but with Li occupying different sites, resulting in a helical Li ion transport tunnel in the framework. Structure type IV, in the $C2/c$ space group, is characteristic of a tubular architecture with Li ions accommodated inside the tubes that provide the diffusion paths.

Extending the subgraphs to a graph distance of four leads to the conclusion that the difference among these structure types lies in the distribution of the second sheath of polyhedra to the central one, as revealed in Figure 2b. We can see the obvious difference among the five structures from the configurations of nodes and edges outside the local atomic environment region (with a graph distance of three, marked by the blue shadow in the insets). While their local atomic environments are identical in topology, the subtle change in the alignment of structure units as indicated by this second sheath of polyhedra will give rise to noticeable changes in Li ion diffusion paths and therefore modulate the ionic conductivity to some extent.

2.3. Favorable Li Diffusion Pathways. The bond-valence site energy (BVSE) method,[35] which has been widely used to identify areas with weak electrostatic interaction in a crystal structure,[36−39] was employed to search for the potential Li diffusion pathways (Figure S1). After that, density functional theory (DFT) calculations using climbing image nudged elastic band (CI-NEB) method[40,41] were conducted to obtain the activation barriers. For all of the structure types, we used the same composition as $LiTi_2(PO_4)_3$ to enable direct comparison between these five structures, without any influence from the constituent elements. The calculated activation barrier for Li diffusion along the most favorable path in each of structure types I−IV is in the range 0.1−0.4 eV (Figure S2), which is comparable to that in $LiTi_2(PO_4)_3$ (0.39 eV). This confirms our assumption that similar topology of local atomic environment can potentially lead to similar activation barrier for Li transport.

We further investigated the Li coordination environments along the diffusion paths according to the CI-NEB calculations.

https://doi.org/10.1021/jacs.4c04202
J. Am. Chem. Soc. 2024, 146, 18535−18543

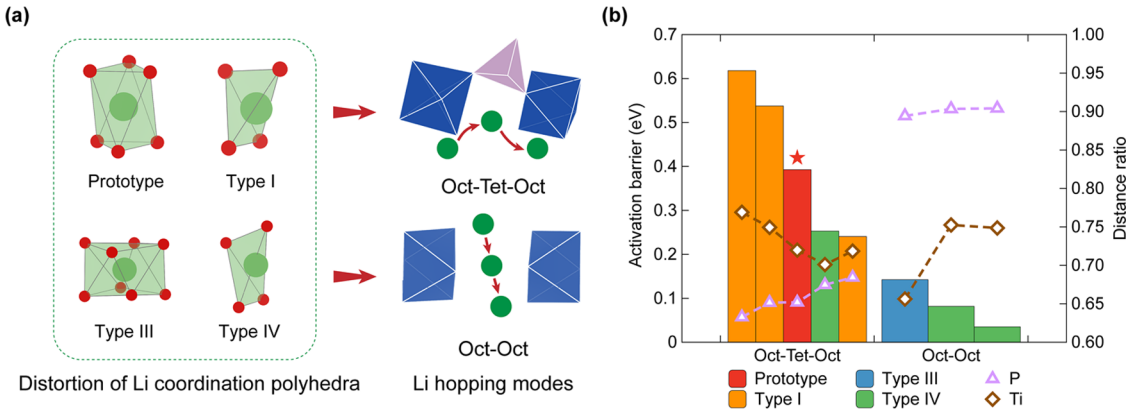

Figure 3. Li coordination environments along the diffusion paths and the corresponding activation barrier. (a) Li environments at the initial state in the $LiTi_2(PO_4)_3$ prototype and structure types I, III, and IV. Two kinds of Li hopping modes (i.e., Oct−Tet−Oct and Oct−Oct) are identified in these structures. (b) Energy barriers for different Li diffusion paths in the prototype and structure types I, III, and IV. The normalized distance ratios between the saddle point location during Li diffusion and the sites of neighboring non-Li cations are also presented (dashed lines).

Previous studies have suggested that the distortion of Li coordination environment is critical for Li transport in a non-Li framework[42] and that the distortion degree of this environment can be well assessed by the continuous symmetry measure (CSM).[43] As shown in Figure 3a, for pristine static configurations, the Li coordination environments in structure types I, III, and IV do not exhibit the octahedral symmetry displayed in the $LiTi_2(PO_4)_3$ prototype. We note that structure type II is not presented here, because it is actually a direct combination between the prototype and structure type I, as discussed above. This means that Li coordination environments in the structure type II are identical to those of either the prototype or type I. Hence, the structure type II is left out of consideration in the following discussion. The CSM values for the prototype and the structure types I, III, and IV are calculated to be 4.82, 6.71, 16.48, and 3.45, respectively, taking the regular tetrahedron, octahedron, and cube as references (i.e., the ideal polyhedral geometry) for coordination numbers of 4, 6, and 8, respectively. The relatively high distortion degree can confer a high lattice energy at the initial state for Li diffusion, which is beneficial for reducing the activation barrier. We have also examined the cases of Li stuffing in structure type I (Figure S4). It turns out that the excess Li ions are accommodated in coordination environments with a similar degree of distortion to that of the pristine structure. This is consistent with the prediction of relatively lower activation barrier for configurations with excess Li ions in the lattice, as shown in Figure S5. We also note that this Li stuffing condition can reduce the disparity between these four structure types regarding the Li diffusion barrier. The fact that the barriers for concerted Li migration in all of these structures are in the range of 0.06−0.25 eV (Figure S5) adds another evidence to our claim that the difference in ion-transport properties could be relatively small for compounds with strong correlation in topology.

Two types of diffusion paths, corresponding to the octahedron−tetrahedron−octahedron (Oct−Tet−Oct) and direct Oct−Oct Li hopping modes, have been identified in the prototype and structure types I, III, and IV (Figure 3a). The former mode requires the motion of Li through a gate site constituted by the edge connections of three polyhedra. In this configuration, the PO_4 tetrahedron causes a deviation of the saddle point location out of the bisecting plane of these octahedra, thus resulting in an S-shaped twisty trajectory for Li diffusion. The latter mode, however, is characterized by a direct, face-sharing alignment of two octahedra without any intervening tetrahedron, thus, enabling a weak interaction of Li ions with the non-Li cations. By subgraph isomorphism analysis, we use the graph edit distance metric, i.e., the number of steps taken to transform a graph into the targeted sample (see details in the Supporting Information), to evaluate the similarity between two structure types. At a graph distance of four, the graph edit distance between the prototype and structure type I is 3, whereas it is 2 between structure types III and IV, as illustrated by the two sets of subgraph patterns depicted in Figure 2b. It means that the prototype and structure type I are similar even in the second sheath of polyhedra, and such high similarity is also demonstrated between structure types III and IV. This result may account for the fact that the prototype and structure type I only contain pathways of Oct−Tet−Oct type, while structure types III and IV have pathways of Oct−Oct type, matching well with their difference in activation barriers (Figure 3b).

To provide a quantitative evaluation of the interaction of Li ions with the non-Li cations during diffusion, we used a metric of normalized distance ratio between the saddle point location of Li diffusion and the sites of neighboring non-Li cations (the detailed method is provided in the Section 5). As shown in Figure 3b, the distance ratio with respect to the P atom is negatively correlated with the activation barrier in an overall trend. In the pathways of Oct−Tet−Oct type, a discernible trend is the smaller distance ratio with respect to Ti atom leading to relatively lower activation barrier. This can be rationalized by the decreased inter-octahedral distance that drives the saddle point location away from the PO_4 tetrahedron. The above analysis underscores that the electrostatic repulsion exerted by the non-Li cations, especially the main group element in the XO_4 tetrahedron, on Li ions during their motion to the saddle point location is of paramount importance for Li conductivity in these structure types.

2.4. Identification of Potential ISSEs. We further screened the database (consisting of 544,145 inorganic compounds) for materials that belong to the structure types I, III, and IV so as to identify candidates suitable as ISSEs. Such material should contain Li, and we also constrained our investigation to compounds with less than 200 atoms in a unit cell so that there is not too much burden in the following DFT calculations. Moreover, we neglected the compounds contain-

https://doi.org/10.1021/jacs.4c04202
J. Am. Chem. Soc. 2024, 146, 18535−18543

ing H atoms because the database entries of these materials generally provide inaccurate information for the coordinates of H (some of them could even be missing). The above criteria lead to a much narrower range of candidate compounds (29,330 entries). Then, we used the subgraph isomorphism matching algorithm for screening and removed all of the duplicate entries via the graph matching scheme proposed in our previous work.[26] This results in a portfolio of 104 materials (listed in Table S1), and the screening flow is shown in Figure S6. Ab initio molecular dynamics (AIMD) simulations were employed to evaluate their ionic conductivity and activation barriers for Li diffusion.

The AIMD calculation results are provided in Figure 4, showing that a large number of compounds exhibit higher

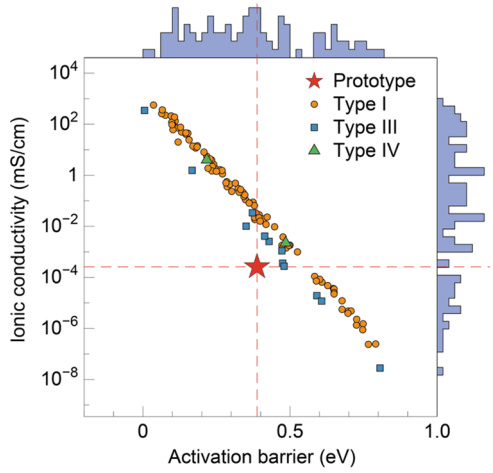

Figure 4. AIMD-calculated ionic conductivity at room temperature and Li diffusion activation barrier for the candidate fast ion conductors identified via subgraph isomorphism matching. The room-temperature ionic conductivity is extrapolated from the calculation results at high temperatures, and the activation barrier is fitted according to the Arrhenius law. The population of materials with a high ionic conductivity and a low activation barrier is illustrated in the frequency distribution histograms.

ionic conductivities than those of the $LiTi_2(PO_4)_3$ prototype. Over three-fourths of the compounds present activation barriers of below 0.5 eV for Li diffusion. These results justify the reliability of using subgraph isomorphism for the identification of potential fast ion conductors. We note that for compounds with exceptionally high activation barriers, the sluggish Li diffusion is mostly due to the complete filling of stable Li sites (generally at high symmetry Wyckoff positions) and the absence of Li ions at less stable sites. This condition confers high stability to the pristine configuration and makes it difficult to activate a Li ion to the metastable sites along the diffusion paths. Accordingly, introducing Li vacancies into the compounds can effectively reduce the activation barriers. Moreover, the fact that $LiTi_2(PO_4)_3$ falls below the trendline of structure types I, III, and IV in Figure 4, indicates a higher pre-exponential factor of these structure types as compared to the prototype. This could be related to the less symmetric and more distorted local atomic environments in structure types I, III, and IV than that of $LiTi_2(PO_4)_3$.

In pursuit of ISSEs, we should take into account other essential attributes such as electronic conductivity and the electrochemical stability window. Here we set a criterion that the electronic band gap should exceed 2 eV. All compounds belonging to structure types III and IV are filtered because their band gaps are almost near zero. We also specify that the electrochemical stability window should exceed 0.5 V. As shown in Figure 5, a total of 13 compounds out of the 104

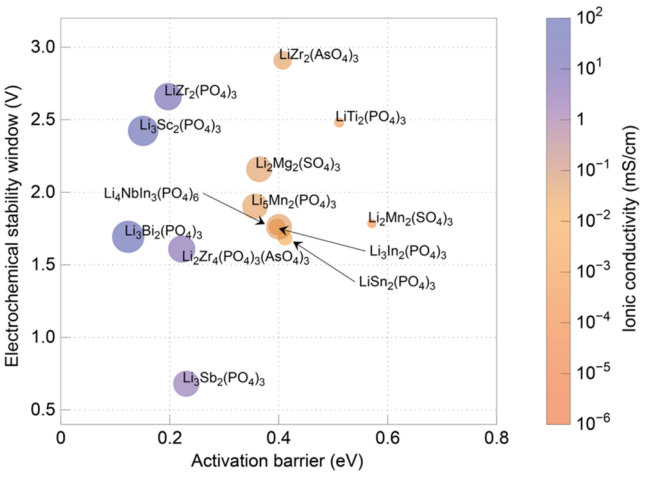

Figure 5. Potential ISSEs identified in this work. A total of 13 compounds are discovered to be electrochemically stable and exhibit low Li diffusion activation barrier and promising ionic conductivity. Ionic conductivity is indicated by the color and size of the circle.

candidates meet both of the above criteria (their structures are shown in Figures S8–S20). Notably, $LiZr_2(AsO_4)_3$ shows the widest electrochemical stability window, along with a Li diffusion activation barrier on par with the $LiTi_2(PO_4)_3$ prototype. Its ionic conductivity can be further modified by partially substituting AsO_4 with PO_4, as demonstrated by the result of $Li_2Zr_4(PO_4)_3(AsO_4)_3$. $Li_2Mg_2(SO_4)_3$ is the most cost-effective candidate, which was also predicted by a previous work to possess appropriate electrochemical stability window and promising ionic conductivity simultaneously.[20] $Li_3Bi_2(PO_4)_3$ exhibits the highest ionic conductivity (52 mS/cm), and its diffusion path is three-dimensional percolating, as shown in Figure S18. We believe that this material is worth the experimental effort in future studies.

3. DISCUSSION

Due to their competitive advantage in air and electrochemical stability over sulfide and halide counterparts, oxide-based ISSEs have attracted extensive research interest since the early discovery of the famous prototype materials including $LiTi_2(PO_4)_3$, $Li_{3x}La_{2/3-x}TiO_3$, $Li_7La_3Zr_2O_{12}$, etc.[44,45] A long-standing challenge lies in achieving a room-temperature conductivity greater than 1 mS/cm, which has been exhibited by only a very limited number of oxide-based ISSEs. As a result, most of previous studies have focused on the modification of the above prototype materials, and many strategies have been proposed to improve the conductivity via control over Li ion content.[46−48] Methods to affect the distortion degree of the rigid framework structures have also been exploited, such as changing the lattice volume,[16] neck size,[17,49] and polyhedral size of non-Li cation.[20,50] These changes will affect the coordination environment of Li ions, typically increasing the energy at stable Li sites and leading to a reduced migration barrier. Despite the advances in this field, it is still difficult to fulfill all of the performance requirements by simple chemical modifications of the existing prototype

https://doi.org/10.1021/jacs.4c04202
J. Am. Chem. Soc. 2024, 146, 18535−18543

materials, whereas more complicated modifications tend to increase the final price, which will inevitably impede their industrial applications. Therefore, there remains a great need to discover new material systems beyond the existing prototypes. While the identification of potential ISSE materials has been previously bottlenecked by a laborious trial-and-error procedure, the recent rapid progress in data-mining techniques offers powerful tools to accelerate the discovery of candidate materials. In the present work, we show that the subgraph isomorphism matching algorithms can be added into the data-mining tool box for the efficient and reliable recommendation of fast ion conductors that could be further employed as ISSEs.

Different from earlier studies that utilized either global factors such as symmetry or key local factors such as the coordination environment of Li to explore previously unknown or overlooked materials for ISSEs, our approach enables a fast screening for topological frameworks that are likely to be ideal for ion conduction. Via subgraph isomorphism matching, crystal structures with a non-Li framework similar to the prototype material can be identified with a nearly negligible computational cost. We have exemplified this with NASICON-type $LiTi_2(PO_4)_3$. Notably, when we eliminate the difference in constituent elements (i.e., the composition is fixed at $LiTi_2(PO_4)_3$), the Li diffusion activation barriers in all of the discovered crystal structures are close to or even lower than that of the prototype material (Figure 3). When we do not remove the influence from the constituent elements (i.e., the compounds with the targeted structure type are extracted from the materials database), the majority of the identified compounds can still exhibit properties similar to those of $LiTi_2(PO_4)_3$ (Figure 4). Especially, over 77% of the identified compounds have an ionic conductivity greater than that of $LiTi_2(PO_4)_3$, and the ionic conductivity for over 37% of the compounds could surpass 1 mS/cm, meaning that our convenient graph-based algorithm can offer high efficiency for navigating the chemical space in search of fast ion conductors.

Another advantage of our approach is that it can be readily adapted to a wide range of prototype materials, even if not limited to those for Li ion batteries. We can expect that a much larger number of candidate materials for ISSEs can be uncovered when the algorithm is applied to other prototypes such as garnet-type oxides as well as some specific sulfide/halide ISSEs that have been reported in recent years. Moreover, the node representation of subgraphs can potentially be extended from atom to polyhedron, through which the subgraphs can describe the spatial arrangement of ordered polyhedra to facilitate the screening of fast ion conductors with separated non-Li cationic polyhedra. Compositional design can be employed to further improve the ionic conductivity of the candidate compounds because our screening method emphasizes the topological structure rather than the material composition. Generally, Li stuffing is an effective compositional design strategy, which causes intensification of Coulomb repulsion, thus activating the concerted migration of multiple Li ions and leading to a reduced migration barrier.[51] For compounds with relatively high Li content, introduction of Li vacancies into the lattice via compositional modulation could be an alternative strategy to enhance ionic conductivity.[52] Actually, from Figure 4, we note that the calculated ionic conductivities can vary several orders of magnitude despite the similar local structures. This could be largely attributed to the difference in Li content for different materials, given that the various elements in the non-Li framework will correspond to a wide range of valence states.

The fact that our approach relies solely on the topology of the framework would suggest that the element-related effects of the framework have been neglected in the calculations. This is a major challenge of nearly all of the structural representations using undirected graphs in materials science. Especially, the information on interatomic distance has not been stored in the subgraph representations in our work, which precludes us from capturing the size effect of the ion diffusion paths.[50] This could be another reason for the large variation of the ionic conductivities shown in Figure 4. Moreover, the configuration of Li ions is also neglected in the algorithm. Specifically, recent studies have demonstrated a close relationship between ion migration and lattice dynamic,[53−55] revealing the predominance of concertation between multiple mobile ions and further elucidating the essential role of ion hopping lengths and hopping spans in the lattice. Although our approach cannot incorporate this collective mechanism for the evaluation of Li ion mobility, the main idea that Li ion diffusion correlates greatly with the rigid topological framework is consistent with these previous works. Furthermore, it is worth noting that apart from the activation energy, the pre-exponential factor could also be an important parameter for ionic conductivity. In this work, materials with the same structure type exhibit similar pre-exponential factors due to the rigid character of the framework structure, which implies that further compositional modification may exert a relatively limited influence on the pre-exponential factor.

Another shortcoming of this graph-based method is that it cannot contain nodes of partial occupancy of non-Li cations at Li sites. We note that the cation-disordered structures (e.g., solid-solution rocksalt compounds)[56−58] have recently gained increasing attention in the field of ISSEs. The disorder at lattice sites that can be assigned to either a Li diffusion tunnel or a non-Li framework precludes us from designating the corresponding subgraphs as subjects for isomorphism matching with another structure. To address this limitation, we may try to consider all of the possible configurations in a given cell size to represent the random distribution of atoms in a disordered material. Apparently, this will lead to a substantial increase in the computation costs. Nevertheless, our scheme of graph representation of local atomic environments can still open up a different avenue from the previous studies that only focused on specific structural characteristics, such as the face-sharing configurations of polyhedra.

4. CONCLUSIONS

Overall, the subgraph isomorphism matching method introduced in this work enables a thorough evaluation of the similarity in topology between the framework structures of the two different compounds. Our screening is based on the assumption that compounds bearing strong resemblance to existing ISSEs are likely to exhibit promising ionic conductivity. Such a resemblance is expected to be more reliant on the local atomic environment than the global features such as lattice symmetry. Since the subgraphs of a crystal structure can well represent the topology of local atomic environments, it is anticipated that if the subgraphs of two structures are isomorphic, their non-Li frameworks tend to be very alike and so does their ionic conductivity. Especially, we find that subgraphs with a graph distance of three can fully incorporate the information on geometry and distribution for each pair of

https://doi.org/10.1021/jacs.4c04202
J. Am. Chem. Soc. 2024, 146, 18535−18543

neighboring polyhedra in the framework. Such subgraphs can thus be employed for isomorphism matching, which will narrow down the search area while not restricting it to a specific compositional range. In this context, we examine the above assumptions by taking the NASICON-type $LiTi_2(PO_4)_3$ as an example, and it turns out that all of the structure types identified via our algorithm demonstrate comparable ionic conductivity to the $LiTi_2(PO_4)_3$ prototype. Moreover, a detailed inspection of the local atomic environments indicates that the distortion of Li coordination polyhedra and the distance from the saddle point location to XO_4 tetrahedra during Li diffusion are the two main factors dictating Li conductivity. By screening the materials database for compounds belonging to the identified structure types, 13 candidates for ISSE have been discovered out of 29,330 inorganic compounds. All of these candidate materials have suitable electronic structure, wide electrochemical stability window, and promising Li conductivity, which demonstrates the efficiency of our algorithm in accelerating the discovery of fast ion conductors for all-solid-state lithium-ion batteries.

5. EXPERIMENTAL SECTION

5.1. Density Functional Theory Calculations. All of the first-principles calculations were performed by the Vienna Ab initio Simulation Package (VASP)[59] with the projector augmented wave (PAW) method and the Perdew−Burke−Ernzerhof (PBE)[60] approximation. A plane wave basis with a cutoff energy of 520 eV was used, and Γ-centered *k*-meshes were selected with the smallest spacing between *k*-points of 0.4 for structural optimization and 0.25 for energy calculations.

5.2. Ab Initio Molecular Dynamics Simulation. A Γ-point-only sampling of *k*-space was used for all AIMD simulations with a time step of 2 fs. The initial structures were relaxed and then heated to the targeted temperature (1200 K) by a velocity scaling over 10 ps. Subsequently, the samples were equilibrated at each temperature point (1000, 1100, and 1200 K) for 20 ps, and the initial 2 ps trajectories were excluded from investigation. For the 13 candidate ISSEs, additional AIMD temperature points (800, 900, 1000, 1100, and 1200 K) were used to obtain more accurate computational results.

5.3. Distance Ratio. A normalized distance ratio was used to quantitatively compare the electrostatic repulsion exerted by the non-Li cations at the saddle point location during Li diffusion. For the Oct−Tet−Oct hopping mode, only the PO_4 that connects two adjacent octahedra near the saddle point location was focused on. Two TiO_6 octahedra that are closest to the saddle point location were also considered. The distance ratio was calculated using the following equation

$$r_d = \frac{1}{N}\sum_j \frac{r_{ji}}{r_c} \quad (1)$$

where N is the number of neighboring non-Li cations for consideration and r_{ji} is the interatomic distance between atom i and j. To compare the relative sizes of distance ratios of different elements, we uniformly set r_c to 4 Å. As the maximum nearest neighbor atomic distances of Ti and P atoms are smaller than 4 Å in all of these structure types with $LiTi_2(PO_4)_3$ composition, r_c was used here to normalize the average distances to a range of 0−1.

5.4. Graph Edit Distance. To quantitatively describe the similarity between different subgraph structures, we employed the metric of graph edit distance, which refers to the number of changes in nodes and edges required to make two graphs isomorphic. A graph edit distance of 1 can be regarded as the addition or deletion of a node or an edge in the subgraph.

5.5. Crystal Structure Data Set. The data set was built in our previous work,[26] with the structure entries extracted from the Inorganic Crystal Structure Database (ICSD),[61] the Open Quantum Materials Database,[62] the Materials Project database,[63] the Crystallography Open Database,[64] and the AFLOW.[65] A total of 544,145 crystal structures were included in the data set.

■ ASSOCIATED CONTENT

Data Availability Statement

All code needed to replicate the results in this work is available from https://github.com/PKUSZSAM/Subgraph_algorithm

Supporting Information

The Supporting Information is available free of charge at https://pubs.acs.org/doi/10.1021/jacs.4c04202.

Details of area−distance pair clustering method, CI-NEB calculations, electrochemical stability calculations, ionic conductivity calculations, graph edit distance calculations, concerted migration calculations, Arrhenius plots, Li ion probability density, electrochemical stability window, and summary of 13 candidate materials (PDF)

■ AUTHOR INFORMATION

Corresponding Authors

Shunning Li − *School of Advanced Materials, Peking University, Shenzhen Graduate School, Shenzhen 518055, P. R. China;* orcid.org/0000-0002-5381-6025; Email: lisn@pku.edu.cn

Feng Pan − *School of Advanced Materials, Peking University, Shenzhen Graduate School, Shenzhen 518055, P. R. China;* orcid.org/0000-0002-8216-1339; Email: panfeng@pkusz.edu.cn

Authors

Wentao Zhang − *School of Advanced Materials, Peking University, Shenzhen Graduate School, Shenzhen 518055, P. R. China*

Mouyi Weng − *School of Advanced Materials, Peking University, Shenzhen Graduate School, Shenzhen 518055, P. R. China; Theory and Simulation of Materials, École Polytechnique Fédérale de Lausanne, Lausanne CH-1015, Switzerland*

Mingzheng Zhang − *School of Advanced Materials, Peking University, Shenzhen Graduate School, Shenzhen 518055, P. R. China*

Zhefeng Chen − *School of Advanced Materials, Peking University, Shenzhen Graduate School, Shenzhen 518055, P. R. China*

Bingxu Wang − *School of Advanced Materials, Peking University, Shenzhen Graduate School, Shenzhen 518055, P. R. China*

Complete contact information is available at: https://pubs.acs.org/10.1021/jacs.4c04202

Notes

The authors declare no competing financial interest.

■ ACKNOWLEDGMENTS

The authors acknowledge financial support from the National Natural Science Foundation of China (22109003), Soft Science Research Project of Guangdong Province (no. 2017B030301013), the Basic and Applied Basic Research Foundation of Guangdong Province (2021B1515130002 and 2023A1515011391), and the Major Science and Technology Infrastructure Project of Material Genome Big-science

Facilities Platform supported by Municipal Development and Reform Commission of Shenzhen.

REFERENCES

(1) Tarascon, J. M.; Armand, M. Issues and Challenges Facing Rechargeable Lithium Batteries. *Nature* **2001**, *414* (6861), 359−367.

(2) Larcher, D.; Tarascon, J. M. Towards Greener and More Sustainable Batteries for Electrical Energy Storage. *Nat. Chem.* **2015**, *7* (1), 19−29.

(3) Wang, Y.; Richards, W. D.; Ong, S. P.; Miara, L. J.; Kim, J. C.; Mo, Y.; Ceder, G. Design Principles for Solid-State Lithium Superionic Conductors. *Nat. Mater.* **2015**, *14* (10), 1026−1031.

(4) Murugan, R.; Thangadurai, V.; Weppner, W. Fast Lithium Ion Conduction in Garnet-Type $Li_7La_3Zr_2O_{12}$. *Angew. Chem., Int. Ed.* **2007**, *46* (41), 7778−7781.

(5) Inaguma, Y.; Liquan, C.; Itoh, M.; Nakamura, T.; et al. High ionic conductivity in lithium lanthanum titanate. *Solid State Commun.* **1993**, *86* (10), 689−693, DOI: 10.1016/0038-1098(93)90841-A.

(6) Bruce, P. G.; West, A. R. The A-C Conductivity of Polycrystalline LISICON, $Li_{2+2x}Zn_{1-x}GeO_4$, and a Model for Intergranular Constriction Resistances. *J. Electrochem. Soc.* **1983**, *130* (3), 662−669.

(7) Feng, Z.; Rajagopalan, R.; Sun, D.; Tang, Y.; Wang, H. In-Situ Formation of Hybrid Li_3PO_4-$AlPO_4$-$Al(PO_3)$ Coating Layer on $LiNi_{0.8}Co_{0.1}Mn_{0.1}O_2$ Cathode with Enhanced Electrochemical Properties for Lithium-Ion Battery. *Chem. Eng. J.* **2020**, *382*, No. 122959.

(8) Qu, X.; Yu, Z.; Ruan, D.; Dou, A.; Su, M.; Zhou, Y.; Liu, Y.; Chu, D. Enhanced Electrochemical Performance of Ni-Rich Cathode Materials with $Li_{1.3}Al_{0.3}Ti_{1.7}(PO_4)_3$ Coating. *ACS Sustainable Chem. Eng.* **2020**, *8* (15), 5819−5830.

(9) Zhang, J.; Zhong, H.; Zheng, C.; Xia, Y.; Liang, C.; Huang, H.; Gan, Y.; Tao, X.; Zhang, W. All-Solid-State Batteries with Slurry Coated $LiNi_{0.8}Co_{0.1}Mn_{0.1}O_2$ Composite Cathode and Li_6PS_5Cl Electrolyte: Effect of Binder Content. *J. Power Sources* **2018**, *391*, 73−79.

(10) Yang, G.; Liang, X.; Zheng, S.; Chen, H.; Zhang, W.; Li, S.; Pan, F. Li-Rich Channels as the Material Gene for Facile Lithium Diffusion in Halide Solid Electrolytes. *eScience* **2022**, *2* (1), 79−86.

(11) Knauth, P. Inorganic Solid Li Ion Conductors: An Overview. *Solid State Ionics* **2009**, *180* (14−16), 911−916.

(12) Zhao, X.; Zhang, Z.; Zhang, X.; Tang, B.; Xie, Z.; Zhou, Z. Computational Screening and First-Principles Investigations of NASICON-Type $Li_xM_2(PO_4)_3$ as Solid Electrolytes for Li Batteries. *J. Mater. Chem. A* **2018**, *6* (6), 2625−2631.

(13) Park, D.; Park, H.; Lee, Y.; Kim, S. O.; Jung, H. G.; Chung, K. Y.; Shim, J. H.; Yu, S. Theoretical Design of Lithium Chloride Superionic Conductors for All-Solid-State High-Voltage Lithium-Ion Batteries. *ACS Appl. Mater. Interfaces* **2020**, *12* (31), 34806−34814.

(14) Wang, S.; Bai, Q.; Nolan, A. M.; Liu, Y.; Gong, S.; Sun, Q.; Mo, Y. Lithium Chlorides and Bromides as Promising Solid-State Chemistries for Fast Ion Conductors with Good Electrochemical Stability. *Angew. Chem., Int. Ed.* **2019**, *58* (24), 8039−8043.

(15) Zhang, B.; Zhong, J.; Zhang, Y.; Yang, L.; Yang, J.; Li, S.; Wang, L. W.; Pan, F.; Lin, Z. Discovering a New Class of Fluoride Solid-Electrolyte Materials via Screening the Structural Property of Li-Ion Sublattice. *Nano Energy* **2021**, *79*, No. 105407.

(16) Xu, Z.; Chen, X.; Chen, R.; Li, X.; Zhu, H. Anion Charge and Lattice Volume Dependent Lithium Ion Migration in Compounds with Fcc Anion Sublattices. *npj Comput. Mater.* **2020**, *6* (1), No. 47, DOI: 10.1038/s41524-020-0324-7.

(17) He, X.; Bai, Q.; Liu, Y.; Nolan, A. M.; Ling, C.; Mo, Y. Crystal Structural Framework of Lithium Super-Ionic Conductors. *Adv. Energy Mater.* **2019**, *9* (43), No. 1902078, DOI: 10.1002/aenm.201902078.

(18) Liu, Y.; Wang, S.; Nolan, A. M.; Ling, C.; Mo, Y. Tailoring the Cation Lattice for Chloride Lithium-Ion Conductors. *Adv. Energy Mater.* **2020**, *10* (40), No. 2002356, DOI: 10.1002/aenm.202002356.

(19) Boyce, J. B.; Huberman, B. A. Superionic Conductors: Transitions, Structures, Dynamics. *Phys. Rep.* **1979**, *51* (4), 189−265.

(20) Jun, K. J.; Sun, Y.; Xiao, Y.; Zeng, Y.; Kim, R.; Kim, H.; Miara, L. J.; Im, D.; Wang, Y.; Ceder, G. Lithium Superionic Conductors with Corner-Sharing Frameworks. *Nat. Mater.* **2022**, *21* (8), 924−931.

(21) Blatov, V. A. Search for Isotypism in Crystal Structures by Means of the Graph Theory. *Acta Crystallogr., Sect. A: Found. Crystallogr.* **2000**, *56* (2), 178−188.

(22) Ong, S. P.; Richards, W. D.; Jain, A.; Hautier, G.; Kocher, M.; Cholia, S.; Gunter, D.; Chevrier, V. L.; Persson, K. A.; Ceder, G. Python Materials Genomics (Pymatgen): A Robust, Open-Source Python Library for Materials Analysis. *Comput. Mater. Sci.* **2013**, *68*, 314−319.

(23) Jian, Z.; Hu, Y. S.; Ji, X.; Chen, W. NASICON-Structured Materials for Energy Storage. *Adv. Mater.* **2017**, *29* (20), No. 1601925, DOI: 10.1002/adma.201601925.

(24) Lang, B.; Ziebarth, B.; Elsässer, C. Lithium Ion Conduction in $LiTi_2(PO_4)_3$ and Related Compounds Based on the NASICON Structure: A First-Principles Study. *Chem. Mater.* **2015**, *27* (14), 5040−5048.

(25) Zhang, B.; Lin, Z.; Dong, H.; Wang, L. W.; Pan, F. Revealing Cooperative Li-Ion Migration in $Li_{1+x}Al_xTi_{2-x}(PO_4)_3$ Solid State Electrolytes with High Al Doping. *J. Mater. Chem. A* **2020**, *8* (1), 342−348.

(26) Weng, M.; Wang, Z.; Qian, G.; Ye, Y.; Chen, Z.; Chen, X.; Zheng, S.; Pan, F. Identify Crystal Structures by a New Paradigm Based on Graph Theory for Building Materials Big Data. *Sci. China Chem.* **2019**, *62* (8), 982−986.

(27) Isayev, O.; Oses, C.; Toher, C.; Gossett, E.; Curtarolo, S.; Tropsha, A. Universal Fragment Descriptors for Predicting Properties of Inorganic Crystals. *Nat. Commun.* **2017**, *8*, No. 15679.

(28) Li, S.; Chen, Z.; Wang, Z.; Weng, M.; Li, J.; Zhang, M.; Lu, J.; Xu, K.; Pan, F. Graph-Based Discovery and Analysis of Atomic-Scale One-Dimensional Materials. *Natl. Sci. Rev.* **2022**, *9*, No. nwac028, DOI: 10.1093/nsr/nwac028.

(29) Zheng, J.; Ye, Y.; Pan, F. Structure Units" as Material Genes in Cathode Materials for Lithium-Ion Batteries. *Natl. Sci. Rev.* **2020**, *7* (2), 242−245.

(30) Patoux, S.; Wurm, C.; Morcrette, M.; Rousse, G.; Masquelier, C. A Comparative Structural and Electrochemical Study of Monoclinic $Li_3Fe_2(PO_4)_3$ and $Li_3V_2(PO_4)_3$. *J. Power Sources* **2003**, *119*−*121*, 278−284.

(31) Manthiram, A.; Goodenough, J. B. Lithium Insertion into $Fe_2(MO_4)_3$ Frameworks: Comparison of M = W with M = Mo. *J. Solid State Chem.* **1987**, *71* (2), 349−360.

(32) Rui, X.; Yan, Q.; Skyllas-Kazacos, M.; Lim, T. M. $Li_3V_2(PO_4)_3$ Cathode Materials for Lithium-Ion Batteries: A Review. *J. Power Sources* **2014**, *258*, 19−38.

(33) Li, G.; Te, L.; Lu, S.; Callaghan, M. P. O.; Lynham, D. R.; Cussen, E. J.; Chen, G. Z. Structure and Ionic-Transport Properties of Lithium-Containing. *Chem. Mater.* **2006**, *18* (10), 4681−4689, DOI: 10.1021/cm060992t.

(34) Thangadurai, V.; Kaack, H.; Weppner, W. J. F. Novel Fast Lithium Conduction in Garnet Type $Li_5La_3M_2O_{12}$ (M = Nb, Ta). *J. Am. Ceram. Soc.* **2003**, *86* (3), 437−440, DOI: 10.1111/j.1151-2916.2003.tb03318.x.

(35) Chen, H.; Wong, L. L.; Adams, S. SoftBV − a Software Tool for Screening the Materials Genome of Inorganic Fast Ion Conductors. *Acta Crystallogr., Sect. B: Struct. Sci., Cryst. Eng. Mater.* **2019**, *75* (1), 18−33.

(36) Zhang, L.; He, B.; Zhao, Q.; Zou, Z.; Chi, S.; Mi, P.; Ye, A.; Li, Y.; Wang, D.; Avdeev, M.; Adams, S.; Shi, S. A Database of Ionic Transport Characteristics for Over 29 000 Inorganic Compounds. *Adv. Funct. Mater.* **2020**, *30* (35), No. 2003087, DOI: 10.1002/adfm.202003087.

(37) He, B.; Chi, S.; Ye, A.; Mi, P.; Zhang, L.; Pu, B.; Zou, Z.; Ran, Y.; Zhao, Q.; Wang, D.; Zhang, W.; Zhao, J.; Adams, S.; Avdeev, M.; Shi, S. High-Throughput Screening Platform for Solid Electrolytes Combining Hierarchical Ion-Transport Prediction Algorithms. *Sci. Data* **2020**, *7* (1), No. 151, DOI: 10.1038/s41597-020-0474-y.

(38) Pan, L.; Zhang, L.; Ye, A.; Chi, S.; Zou, Z.; He, B.; Chen, L.; Zhao, Q.; Wang, D.; Shi, S. Revisiting the Ionic Diffusion Mechanism in Li_3PS_4 via the Joint Usage of Geometrical Analysis and Bond Valence Method. *J. Materiomics* **2019**, *5* (4), 688−695.
(39) He, B.; Mi, P.; Ye, A.; Chi, S.; Jiao, Y.; Zhang, L.; Pu, B.; Zou, Z.; Zhang, W.; Avdeev, M.; Adams, S.; Zhao, J.; Shi, S. A Highly Efficient and Informative Method to Identify Ion Transport Networks in Fast Ion Conductors. *Acta Mater.* **2021**, *203*, No. 116490.
(40) Henkelman, G.; Uberuaga, B. P.; Jonsson, H. Nudged_Elastic Bands. *J. Chem. Phys.* **2000**, *113* (22), 9901−9904.
(41) Mills, G.; Jónsson, H.; Schenter, G. K. Reversible Work Transition State Theory: Application to Dissociative Adsorption of Hydrogen. *Surf. Sci.* **1995**, *324* (2−3), 305−337.
(42) Xiao, Y.; Jun, K.; Wang, Y.; Miara, L. J.; Tu, Q.; Ceder, G. Lithium Oxide Superionic Conductors Inspired by Garnet and NASICON Structures. *Adv. Energy Mater.* **2021**, *11*, No. 2101437.
(43) Di Stefano, D.; Miglio, A.; Robeyns, K.; Filinchuk, Y.; Lechartier, M.; Senyshyn, A.; Ishida, H.; Spannenberger, S.; Prutsch, D.; Lunghammer, S.; Rettenwander, D.; Wilkening, M.; Roling, B.; Kato, Y.; Hautier, G. Superionic Diffusion through Frustrated Energy Landscape. *Chem* **2019**, *5* (9), 2450−2460.
(44) Janek, J.; Zeier, W. G. Challenges in Speeding up Solid-State Battery Development. *Nat. Energy* **2023**, *8*, 230−240.
(45) Kim, K. J.; Balaish, M.; Wadaguchi, M.; Kong, L.; Rupp, J. L. M. Solid-State Li−Metal Batteries: Challenges and Horizons of Oxide and Sulfide Solid Electrolytes and Their Interfaces. *Adv. Energy Mater.* **2021**, *11* (1), No. 2002689, DOI: 10.1002/aenm.202002689.
(46) Gromov, O. G.; Kunshina, G. B.; Kuz'min, A. P.; Kalinnikov, V. T. Ionic Conductivity of Solid Electrolytes Based on $Li_{1.3}Al_{0.3}Ti_{1.7}(PO_4)_3$. *Russ. J. Appl. Chem.* **1996**, *69* (3), 385−388.
(47) Xiong, S.; He, X.; Han, A.; Liu, Z.; Ren, Z.; McElhenny, B.; Nolan, A. M.; Chen, S.; Mo, Y.; Chen, H. Computation-Guided Design of $LiTaSiO_5$, a New Lithium Ionic Conductor with Sphene Structure. *Adv. Energy Mater.* **2019**, *9* (22), No. 1803821, DOI: 10.1002/aenm.201803821.
(48) Samson, A. J.; Hofstetter, K.; Bag, S.; Thangadurai, V. A Bird's-Eye View of Li-Stuffed Garnet-Type $Li_7La_3Zr_2O_{12}$ Ceramic Electrolytes for Advanced All-Solid-State Li Batteries. *Energy Environ. Sci.* **2019**, *12* (10), 2957−2975.
(49) Martínez-Juárez, A.; Pecharromán, C.; Iglesias, J. E.; Rojo, J. M. Relationship between Activation Energy and Bottleneck Size for Li^+ Ion Conduction in NASICON Materials of Composition $LiMM'(PO_4)_3$; M, M′ = Ge, Ti, Sn, Hf. *J. Phys. Chem. B* **1998**, *102* (2), 372−375.
(50) Chen, C. H.; Du, J. Lithium Ion Diffusion Mechanism in Lithium Lanthanum Titanate Solid-State Electrolytes from Atomistic Simulations. *J. Am. Ceram. Soc.* **2015**, *98* (2), 534−542.
(51) He, X.; Zhu, Y.; Mo, Y. Origin of Fast Ion Diffusion in Super-Ionic Conductors. *Nat. Commun.* **2017**, *8*, No. 15893, DOI: 10.1038/ncomms15893.
(52) Stegmaier, S.; Voss, J.; Reuter, K.; Luntz, A. C. Li^+ Defects in a Solid-State Li Ion Battery: Theoretical Insights with a Li_3OCl Electrolyte. *Chem. Mater.* **2017**, *29* (10), 4330−4340.
(53) López, C.; Emperador, A.; Saucedo, E.; Rurali, R.; Cazorla, C. Universal Ion-Transport Descriptors and Classes of Inorganic Solid-State Electrolytes. *Mater. Horiz.* **2023**, *10* (5), 1757−1768.
(54) Muy, S.; Schlem, R.; Shao-Horn, Y.; Zeier, W. G. Phonon−Ion Interactions: Designing Ion Mobility Based on Lattice Dynamics. *Adv. Energy Mater.* **2021**, *11* (15), No. 2002787, DOI: 10.1002/aenm.202002787.
(55) López, C.; Rurali, R.; Cazorla, C. How Concerted Are Ionic Hops in Inorganic Solid-State Electrolytes? *J. Am. Chem. Soc.* **2024**, *146* (12), 8269−8279.
(56) Chen, Y.; Lun, Z.; Zhao, X.; Koirala, K. P.; Li, L.; Sun, Y.; O'Keefe, C. A.; Yang, X.; Cai, Z.; Wang, C.; Ji, H.; Grey, C. P.; Ouyang, B.; Ceder, G. Unlocking Li Superionic Conductivity in Face-Centred Cubic Oxides via Face-Sharing Configurations. *Nat. Mater.* **2024**, *23* (4), 535−542.
(57) Satya Kishore, M. V. V. M.; Marinel, S.; Pralong, V.; Caignaert, V.; D'Astorg, S.; Raveau, B. The Rock Salt Oxide Li_2MgTiO_4: Type I Dielectric and Ionic Conductor. *Mater. Res. Bull.* **2006**, *41* (7), 1378−1384.
(58) McLaren, V. L.; Kirk, C. A.; Poisot, M.; Castellanos, M.; West, A. R. Li^+ Ion Conductivity in Rock Salt-Structured Nickel-Doped Li_3NbO_4. *Dalton Trans.* **2004**, *19*, 3042−3047.
(59) Kresse, G.; Furthmüller, J. Efficient Iterative Schemes for Ab Initio Total-Energy Calculations Using a Plane-Wave Basis Set. *Phys. Rev. B: Condens. Matter Mater. Phys.* **1996**, *54* (16), 11169−11186.
(60) Perdew, J. P.; Ernzerhof, M.; Burke, K. Rationale for Mixing Exact Exchange with Density Functional Approximations. *J. Chem. Phys.* **1996**, *105* (22), 9982−9985.
(61) Belsky, A.; Hellenbrandt, M.; Karen, V. L.; Luksch, P. New Developments in the Inorganic Crystal Structure Database (ICSD): Accessibility in Support of Materials Research and Design. *Acta Crystallogr., Sect. B: Struct. Sci.* **2002**, *58* (3 Part 1), 364−369.
(62) Saal, J. E.; Kirklin, S.; Aykol, M.; Meredig, B.; Wolverton, C. Materials Design and Discovery with High-Throughput Density Functional Theory: The Open Quantum Materials Database (OQMD). *JOM* **2013**, *65* (11), 1501−1509.
(63) Jain, A.; Ong, S. P.; Hautier, G.; Chen, W.; Richards, W. D.; Dacek, S.; Cholia, S.; Gunter, D.; Skinner, D.; Ceder, G.; Persson, K. A. Commentary: The Materials Project: A Materials Genome Approach to Accelerating Materials Innovation. *APL Mater.* **2013**, *1* (1), No. 011002, DOI: 10.1063/1.4812323.
(64) Gražulis, S.; Daškevič, A.; Merkys, A.; Chateigner, D.; Lutterotti, L.; Quirós, M.; Serebryanaya, N. R.; Moeck, P.; Downs, R. T.; Le Bail, A. Crystallography Open Database (COD): An Open-Access Collection of Crystal Structures and Platform for World-Wide Collaboration. *Nucleic Acids Res.* **2012**, *40* (D1), 420−427.
(65) Curtarolo, S.; Setyawan, W.; Hart, G. L. W.; Jahnatek, M.; Chepulskii, R. V.; Taylor, R. H.; Wang, S.; Xue, J.; Yang, K.; Levy, O.; Mehl, M. J.; Stokes, H. T.; Demchenko, D. O.; Morgan, D. AFLOW: An Automatic Framework for High-Throughput Materials Discovery. *Comput. Mater. Sci.* **2012**, *58*, 218−226.